The Interplay between Localized and Propagating Plasmonic Excitations Tracked in Space and Time

Christoph Lemke,*,[†] Till Leißner,[†] Andrey Evlyukhin,[‡] Jörn W. Radke,[†] Alwin Klick,[†] Jacek Fiutowski,[§] Jakob Kjelstrup-Hansen,[§] Horst-Günter Rubahn,[§] Boris N. Chichkov,[‡] Carsten Reinhardt,[‡] and Michael Bauer[†]

[†]Institut für Experimentelle und Angewandte Physik, Christian-Albrechts-Universität zu Kiel, Leibnizstraße 19, D-24118 Kiel, Germany

[‡]Laser Zentrum Hannover e.V., Hollerithallee 8, D-30419 Hannover, Germany

[§]Mads Clausen Institute, NanoSYD, University of Southern Denmark, Alsion 2, DK-6400 Sønderborg, Denmark

Ⓢ *Supporting Information*

ABSTRACT: In this work, the mutual coupling and coherent interaction of propagating and localized surface plasmons within a model-type plasmonic assembly is experimentally demonstrated, imaged, and analyzed. Using interferometric time-resolved photoemission electron microscopy the interplay between ultrashort surface plasmon polariton wave packets and plasmonic nanoantennas is monitored on subfemtosecond time scales. The data reveal real-time insights into dispersion and localization of electromagnetic fields as governed by the elementary modes determining the functionality of plasmonic operation units.

KEYWORDS: Plasmon coupling, plasmonic devices, femtosecond phenomena, nanooptics and surface photoemission
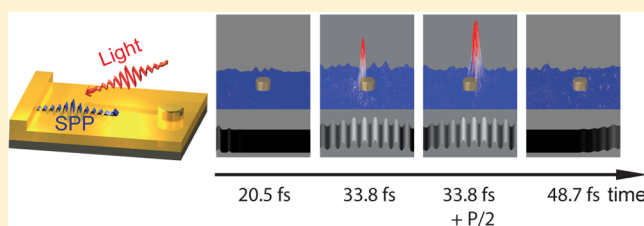
The unique properties of localized surface plasmons (LSPs) and propagating surface plasmon polaritons (SPPs) permitting subwavelength confinement,[1] light velocity propagation, and highly localized sensing[2] are the key features for combining broadband optics and nanoscale electronics.[3−5] As a vision for potential applications, plasmon-based devices could be utilized in future generation on-chip communication and signal processing.[6−8] Because of these prospects, broadband plasmonic excitations and their interaction with nanoscale systems have attracted considerable interest including aspects such as coherence and nonlinearities in localized plasmonic excitations,[9−12] manipulation of plasmonic nearfields by means of pulse shaping techniques,[13] plasmon wave packet propagation along metal−dielectric interfaces,[14−17] and plasmonic coupling to quantum emitters.[18,19] These kinds of studies were accompanied by the development of new instruments, which allow for real-time imaging of ultrafast plasmonic processes with nanometer resolution.[15,20,21] Despite this progress, very fundamental processes such as the interaction between elementary surface plasmonic excitations have barely been investigated so far[22] and there is a particular lack of experimental studies addressing the relevant time- and length scales of such interaction scenarios.

In this work, a model-type coherent interaction scenario between the two elementary plasmonic excitations (LSP and SPP) of relevance for the operation of broadband nano-optical devices is studied with high spatial resolution on a subfemto-second time scale, using interferometric time-resolved two-photon photoemission electron microscopy (ITR-2PPEEM).[10,20] Operation of the experiment in a counter-propagating mode[20] is hereby the vital ingredient as it allows for efficient time-domain discrimination required to distinguish the relevant interaction steps. A plasmonic assembly appropriate for the real-time imaging of LSP-SPP interaction by means of ITR-2PPEEM is schematically illustrated in Figure 1a together with a scanning electron microscope (SEM) image of the real structure under investigation (Figure 1b). It is composed of a gold step edge acting as coupling unit for laser excitation of ultrashort SPP wave packets, a gold-vacuum transmission area for SPP wave packet transportation, and gold nanodots (diameter ≈ 500 nm) acting as LSP antennas for SPP reception and emission. The structured gold film (thickness 120 nm) forming the step and nanodots was prepared by standard electron-beam lithography techniques on top of a continuous, 120 nm thick gold film with a titanium adhesion layer (thickness ≈ 3 nm) supported by a silicon substrate.

For in-operando characterization of the plasmonic assembly on the relevant length and time scales, a photoemission electron microscope operated in the counter-propagating interferometric time-resolved mode was used. Eighteen femtosecond laser pulses at a wavelength of 815 nm delivered from a Ti:sapphire oscillator (Griffin, KMLabs) were used for plasmon
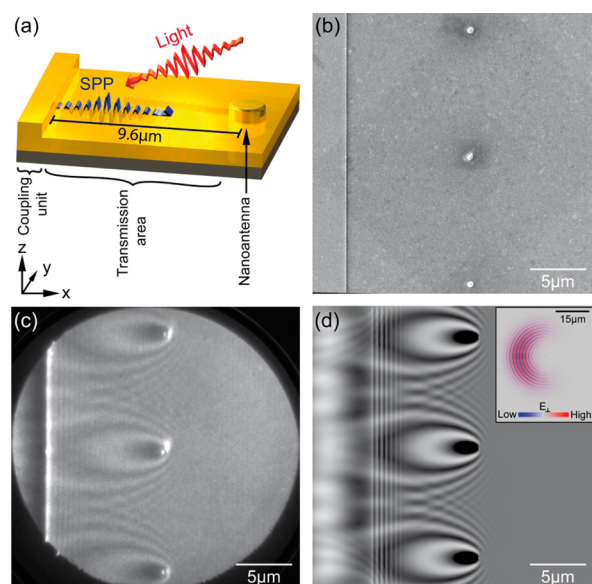
Figure 1. Plasmonic assembly investigated in this work. (a) Schematic illustration of the assembly geometry; the different plasmonic active subunits are indicated. (b) SEM image of the structure; the field of view covers a step edge in the gold film to the left and three gold nanodots in the center functioning as antennas for SPP signal emission and reception. (c) Static 2PPEEM image of the device area shown in (b) recorded at illumination with 18 fs infrared laser pulses incident from the right-hand side. (d) Simulation of the 2PPEEM intensity pattern of the device under consideration of Huygens principle for SPP excitation; the inset shows a snapshot of the SPP polarization field 25 fs after excitation by the laser pulse emerging from an individual gold nanodot as reconstructed from the Huygens simulations.

excitation as well as plasmon tracking via two-photon photoemission (2PPEEM). In order to facilitate two-photon photoemission at $\lambda = 815$ nm, the work function of the plasmonic assembly was lowered to a value below 3 eV by covering it under ultrahigh vacuum conditions with a small amount of Cesium (coverage ≪1 atomic layer) prior to the 2PPEEM experiments.[16] Prior 2PPEEM experiments have shown that in this coverage regime the plasmonic response of the system is not affected within the sensitivity of our experiments.[23] More details of the experimental setup are described in.[20]

The experimental results are supported by theoretical multipole considerations based on the method of decomposed discrete dipole approximation (DDDA) that combines the ordinary discrete dipole approximation with calculations of multipole moments of electric dipole systems.[24] Details of this method for scatterers located on or near a flat metal surface can be found elsewhere.[25] Additionally, simulation of SPP-LSP coupling were performed within the framework of the finite-difference time-domain (FDTD) method, which has been demonstrated to accurately model plasmonic excitations.[16,26−29] The FDTD simulations were performed using the 3D Maxwell solver FullWave from RSoft Design Group.

Figure 1c shows a static two-photon photoemission electron microscopy (2PPEEM) image of the plasmonic structure at illumination with 18 fs, p-polarized laser pulses incident at $\delta = 65°$ incident angle from the right-hand side. The additional image contrast not present in the SEM image results from direct coupling of the laser pulses to the different types of plasmonic modes supported by the assembly subunits.

The periodic intensity patterns in Figure 1c emerging into the gold-vacuum transmission area are the nonlinear photoelectron emission signals associated with SPPs generated by laser coupling at the step edge and the nanodots, respectively. The signals result from alternating constructive and destructive superposition of the laser field with phase-coupled SPPs.[15,20] The interpretation is confirmed by 2PPEEM pattern simulations shown in Figure 1d where a Huygens based approach[16] accounts for SPP excitation at step edge and nanodots, respectively. According to reference data[23,30] a SPP propagation length $L_{SPP} = 62$ μm was used in this simulations, corresponding to a SPP decay time of ∼220 fs. The quantitative analysis of the vertical interference pattern next to the step edge yields the emission of plane SPP wave packets with a center wavelength of 800 ± 2 nm and a pulse width of 18 ± 2 fs. The elliptic shaped pattern results from interference of SPP wave packets emerging from the nanodots (see inset of Figure 1d) with the light, similar to findings for light scattering from micrometer-sized particles.[31] These calculations were performed using analytic expression for SPP radiation fields generated by dipole emitters as reported in reference.[32] Notably, the characteristic angular dependence of the SPP pattern amplitude, in particular the distinct intensity minimum to the right of the nanoantennas, can only be reproduced if the excitation of in-plane as well as out-of-plane dipolar components at the nanoantenna position is taken into account. The main focus, however, is set on the two-lobe electron emission pattern directly at the nanodot position, representing the localized plasmon. Notably, the axis of the two-lobe electron emission structure is oriented parallel to the laser polarization and can be explained if a dipolar characteristic of the particle LSP is taken into account.

The characteristic emission patterns are demonstrated for p-polarized (Figures 1c and 2a) and for s-polarized (Figure 2b)
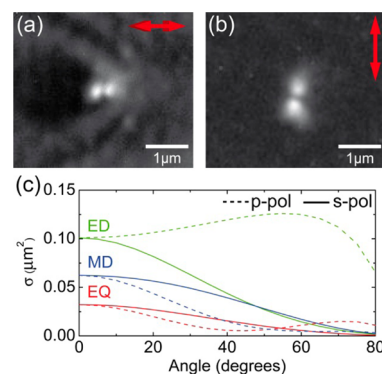

Figure 2. Laser-induced LSP excitation at the gold nanodot. (a) Lower gold nanodot of Figure 1b imaged in 2PPEEM at illumination with (a) p-polarized laser pulses and (b) s-polarized laser-pulses. (c) Results of DDDA calculation on the multipolar character of the LSP for p- and s-polarized laser excitation. The DDDA simulation reveals contributions of the electric dipole (ED), magnetic dipole (MD), and electric quadrupole (EQ) of the gold nanodot to the scattering cross-section σ for different incident angles of the exciting laser pulse.

laser light. The dipolar emission pattern from the nanodots indicates an in-plane component of the LSP. The characteristic SPP emission pattern for p-polarized excitation on the other hand is also indicative for the presence of out-of-plane LSP components.[32] Insight into the individual multipole moments of the LSP excitation is obtained by numerical simulations

using the DDDA. The simulation for p-polarized excitation, shown in Figure 2c, yields a considerable contribution from the electric dipole components at large incident angles whereas higher multipoles can be neglected. For s-polarization, both electric and magnetic dipole moments are excited at large incident angles. In this case, the magnetic dipole moment is excited by the out-of-plane component of the magnetic field of the incident light.

The temporal evolution of the plasmonic fields after laser excitation is revealed within a two-pulse correlation experiment using ITR-2PPEEM. It allows monitoring in real-time SPP propagation and SPP-LSP interaction. The complete ITR-2PPEEM movie made from the assembly and discussed in detail in the following is added to the Supporting Information SI1.

Figure 3 compares ITR-2PPEEM images for two different times t after emission of the SPP wave packet at the step edge. t
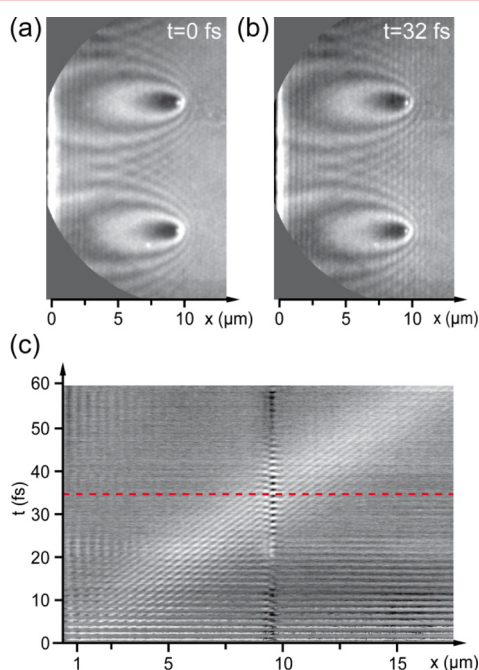

Figure 3. SPP propagation along the transmission area. (a,b) ITR-2PPEEM intensity profiles of SPP propagation recorded at (a) $t = 0$ fs and (b) $t = 32$ fs after emission of the SPP. (c) Space-time representation of SPP propagation along the device transmission area. The SPP propagation signal shows up as diagonal interference pattern. The distortion at a distance $x = 9.6$ μm arises from the interaction between SPP and gold nanodot. The red line indicates t_0, the time at which the SPP envelope maximum arrives at the nanodot position.

refers here to the real-time of SPP propagation in positive x-direction. Because of the non-normal illumination geometry of the experiment, t does not conform to the time-delay ΔT between excitation and probing laser pulse but can be calculated via the relation $t = \Delta T(1 + \sin \delta((v_{g,SPP})/c))^{-1}$, with $v_{g,SPP}$ being the SPP group velocity at a gold–vacuum interface[20] and c is the vacuum speed of light. At $t = 0$ fs (Figure 3a), the ITR-2PPEEM experiment probes the launch of the SPP wave packet from the step edge. Figure 3b shows an ITR-2PPEEM image recorded at $t = 32$ fs, where an additional periodic intensity pattern shows up at a distance of ~9 μm from the step edge. It is the signal of the SPP wave packet that has propagated along the transmission area toward the nanodots. A

comprehensive view onto SPP propagation is provided by the time-space representation shown in Figure 3c. Noticeable is a distortion of the propagation signal at a distance $x = 9.6$ μm from the step edge. It is indicative for the impact of the SPP with the nanodots after the total wave packet transit time $t_0 = 34.5 \pm 1.5$ fs.

The spatiotemporally resolved interaction of the SPP with the nanodots can now be quantified by analysis of experimental ITR-2PPEEM data around t_0 at a nanodot position as shown in Figure 4a–d. The bottom of each figure shows the SPP wave
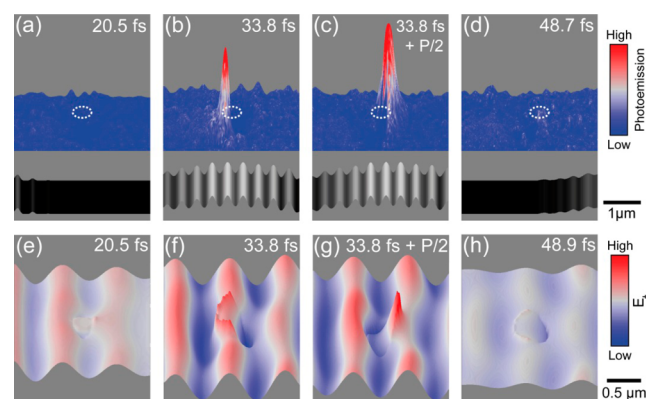

Figure 4. Nanodot excitation via SPP coupling recorded in real time. (a–d) Three-dimensional representation of ITR-2PPEEM close-ups of the center gold nanodot in Figure 1, (a) right before, (b,c) during, and (d) right after the SPP passes the nanodot. In order to derive the pure SPP-related response, the experimental data are background corrected for the static 2PPEEM signal (see Figure 1c). The dotted circle indicates the position of the gold nanodot. In the bottom area of the close-ups integrated ITR-2PPEEM data of the SPP signal (excluding signal contributions from the nanodots) are shown for reference. (e–h) FDTD simulation of SPP-LSP coupling for different times t corresponding to the snap shots shown in (a–d). The images display the electric field amplitude oriented parallel to the surface normal $E_\perp$.

packet signal derived from the experimental propagation data. A response of the nanodot is only observed during the transit of the SPP wave packet (see also movie SI2 in the Supporting Information). Similar to the laser field, the SPP drives a LSP mode of the nanodot with lobe maxima conforming in their position with the static 2PPEEM data at illumination with p-polarized laser light (see Figure 2a). The two lobe maxima oscillate out of phase at an oscillation period $P = 2.7$ fs. Additionally the data demonstrate the feasibility of coherently controlling localized plasmonic fields and subsequent electron emission by the time-delayed interaction of SPP and LSP excitations.

The photoemission pattern transients of SPP-LSP interaction are further supported by FDTD simulations performed under consideration of the experimental assembly and excitation parameters. Simulation snapshots in correspondence to the experimental data in Figure 4a–d are shown in Figure 4e–h. In accordance with the experiment, the calculations show a dipolar oscillatory behavior at a period $P = 2.7$ fs with electric field maxima at the edges of the cylindrical nanodot. Notably, the left–right asymmetry in the simulated electric field response is also observed in the experiment for all three nanodots within the field of view. DDDA calculations indicate that the nanoantenna response to the SPP excitation arises once again from a predominant superposition of in-plane and out-of-plane dipolar LSP modes.

The decay of the LSP is governed by coupling to the radiation far field[33] as well as coupling to the SPP continuum surrounding the nanodots. The comparison of the local LSP signal with simulated ITR-2PPEEM data as shown in Figure 5a
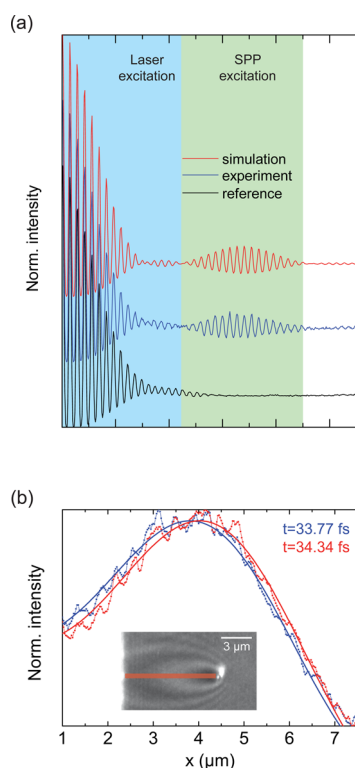

Figure 5. LSP damping via coupling to the SPP continuum. (a) Comparison of experimental and simulated ITR-2PPEEM transients at the nanodot position (left lobe). The blue line corresponds to experimental data; the red line corresponds to simulated data under consideration of rapid LSP decay and transform-limited pulses as given by the Fourier-transform of the experimental laser pulse-spectrum. For reference, the black line shows an interferometric second order laser autocorrelation as determined from the integral 2PPE signal of the flat gold area next to the gold nanodots. The interferometric signal around time-zero shows the LSP response to direct laser excitation, the signal between 50 and 90 fs time-delay is due to SPP-LSP coupling. (b) Experimental evidence for LSP coupling into the SPP continuum provided by the SPP transmission area. The graph compares 2PPE intensity profiles along the red line indicated in the inset at t = 33.77 fs (blue) and t = 34.34 fs (red). The dashed lines are experimental data, the solid lines are results of time-dependent Huygens-simulations. The high-frequency modulations in the experimental data are signatures of the SPP polarization field excited at the coupling unit, not considered in the simulations.

indicates that these damping channels are highly efficient, as the LSP response of the nanodot follows the SPP excitation instantaneously and without any evidence for a postpulse oscillation. Notably, a quantitative agreement between experiment and simulation in the subtle details at time delays between 25 and 45 fs is only achieved if effects of SPP waves emitted at laser excitation from the neighboring nanoantennas are taken into account. Even more, the LSP decay into the SPP continuum directly shows up in the ITR-2PPEEM data and is evidenced by a periodic shift of the elliptic shaped intensity pattern right when the incident SPP wave packet passes the nanodots (see times t between 25 and 45 fs in the Supporting Information movie SI1). Figure 5b provides experimental

photoemission intensity profiles of the elliptic pattern maximum next to the nanodot at t = 33.77 fs and t = 34.34 fs, (dotted lines) in comparison to results from time-dependent Huygens-simulations (solid lines). The quantitative agreement between experimental and simulated data is indeed only achieved if a LSP-clocked emission into concentric SPP waves from the nanodot is considered in the simulation, corroborating the relevance of this SPP channel for the decay of the LSP.

In summary, the application of the ITR-2PPEEM technique together with different simulation strategies enables real-time and comprehensive studies of the action and interaction of different types of fundamental excitations in a plasmonic assembly during ultrafast operation. The analysis of the data provided direct and quantitative information on aspects such as signal transport, plasmon−plasmon coupling, the relevance of loss channels, and the coherent control over the localized plasmonic fields at the nanodot. Implementation of advanced operation units such as plasmon-optical steering components,[34] plasmonic waveguides,[35] or integrated plasmonic characterization tools[36] will in the future further extend the complexity of surface plasmonic interaction processes to be investigated. The sub-5 nm spatial and subfemtosecond temporal resolution capabilities provided by state-of-the-art PEEM instruments even envisions the prospect of addressing ultrafast interaction processes in quantum-plasmonic systems.

■ ASSOCIATED CONTENT

Ⓢ Supporting Information

The complete ITR-2PPEEM movie made from the plasmonic assembly is available as an .avi movie. The background subtracted ITR-2PPEEM measurement, shown for selected temporal delays in Figure 4, is also added as an .avi movie. This material is available free of charge via the Internet at http://pubs.acs.org.

■ AUTHOR INFORMATION

Corresponding Author
*E-mail: lemke@physik.uni-kiel.de.
Notes
The authors declare no competing financial interest.

■ ACKNOWLEDGMENTS

■ REFERENCES

(1) Gramotnev, D. K.; Bozhevolnyi, S. I. *Nat. Photonics* **2010**, *4*, 83−91.
(2) Anker, J. N.; Hall, W. P.; Lyandres, O.; Shah, N. C.; Zhao, J.; Van Duyne, R. P. *Nat. Mater.* **2008**, *7*, 442−53.
(3) Kauranen, M.; Zayats, A. V. *Nat. Photonics* **2012**, *6*, 737−748.
(4) Liu, N.; Wen, F.; Zhao, Y.; Wang, Y.; Nordlander, P.; Halas, N. J.; Alù, A. *Nano Lett.* **2013**, *13*, 142−7.
(5) Halas, N. J. *Nano Lett.* **2010**, *10*, 3816−22.

(6) MacDonald, K. F.; Sámson, Z. L.; Stockman, M. I.; Zheludev, N. I. *Nat. Photonics* **2008**, *3*, 55−58.

(7) Cao, L.; Brongersma, M. L. *Nat. Photonics* **2009**, *3*, 12−13.

(8) Kriesch, A.; Burgos, S. P.; Ploss, D.; Pfeifer, H.; Atwater, H. a; Peschel, U. *Nano Lett.* **2013**, *13*, 4539−45.

(9) Hentschel, M.; Utikal, T.; Giessen, H.; Lippitz, M. *Nano Lett.* **2012**, *12*, 3778−82.

(10) Kubo, A.; Onda, K.; Petek, H.; Sun, Z.; Jung, Y. S.; Kim, H. K. *Nano Lett.* **2005**, *5*, 1123−7.

(11) Stockman, M. I.; Kling, M. F.; Kleineberg, U.; Krausz, F. *Nat. Photonics* **2007**, *1*, 539−544.

(12) Schertz, F.; Schmelzeisen, M.; Mohammadi, R.; Kreiter, M.; Elmers, H.-J.; Schönhense, G. *Nano Lett.* **2012**, *12*, 1885−90.

(13) Aeschlimann, M.; Bauer, M.; Bayer, D.; Brixner, T.; García de Abajo, F. J.; Pfeiffer, W.; Rohmer, M.; Spindler, C.; Steeb, F. *Nature* **2007**, *446*, 301−4.

(14) Rewitz, C.; Keitzl, T.; Tuchscherer, P.; Huang, J.-S.; Geisler, P.; Razinskas, G.; Hecht, B.; Brixner, T. *Nano Lett.* **2012**, *12*, 45−9.

(15) Kubo, A.; Pontius, N.; Petek, H. *Nano Lett.* **2007**, *7*, 470−5.

(16) Lemke, C.; Schneider, C.; Leißner, T.; Bayer, D.; Radke, J. W.; Fischer, A.; Melchior, P.; Evlyukhin, A. B.; Chichkov, B. N.; Reinhardt, C.; Bauer, M.; Aeschlimann, M. *Nano Lett.* **2013**, *13*, 1053−8.

(17) Ropers, C.; Neacsu, C. C.; Elsaesser, T.; Albrecht, M.; Raschke, M. B.; Lienau, C. *Nano Lett.* **2007**, *7*, 2784−8.

(18) Vasa, P.; Wang, W.; Pomraenke, R.; Lammers, M.; Maiuri, M.; Manzoni, C.; Cerullo, G.; Lienau, C. *Nat. Photonics* **2013**, *7*, 128−132.

(19) Gruber, C.; Trügler, A.; Hohenau, A.; Hohenester, U.; Krenn, J. R. *Nano Lett.* **2013**, *13*, 4257−62.

(20) Lemke, C.; Leißner, T.; Jauernik, S.; Klick, A.; Fiutowski, J.; Kjelstrup-Hansen, J.; Rubahn, H.; Bauer, M. *Opt. Express* **2012**, *20*, 12877.

(21) Balistreri, M. L.; Gersen, H.; Korterik, J. P.; Kuipers, L.; van Hulst, N. F. *Science* **2001**, *294*, 1080−2.

(22) Kubo, A.; Jung, Y. S.; Kim, H. K.; Petek, H. *J. Phys. B: At. Mol. Opt. Phys.* **2007**, *40*, S259−S272.

(23) Lemke, C.; Leißner, T.; Klick, A.; Fiutowski, J.; Radke, J. W.; Thomaschewski, M.; Kjelstrup-Hansen, J.; Rubahn, H.-G.; Bauer, M. *Appl. Phys. B: Laser Opt.* **2013**, DOI: 0.1007/s00340-013-5737-2.

(24) Evlyukhin, A. B.; Reinhardt, C.; Chichkov, B. N. *Phys. Rev. B* **2011**, *84*, 235429.

(25) Evlyukhin, A. B.; Reinhardt, C.; Evlyukhin, E.; Chichkov, B. N. *J. Opt. Soc. Am. B* **2013**, *30*, 2589.

(26) Dikken, D. J.; Spasenović, M.; Verhagen, E.; van Oosten, D.; Kuipers, L. K. *Opt. Express* **2010**, *18*, 16112−9.

(27) Bozhevolnyi, S. I. *Opt. Express* **2006**, *14*, 9467−76.

(28) Passinger, S.; Seidel, A.; Ohrt, C.; Reinhardt, C.; Stepanov, A.; Kiyan, R.; Chichkov, B. *Opt. Express* **2008**, *16*, 14369−79.

(29) Zhang, L.; Kubo, A.; Wang, L.; Petek, H.; Seideman, T. *Phys. Rev. B* **2011**, *84*, 245442.

(30) Olmon, R.; Slovick, B.; Johnson, T.; Shelton, D.; Oh, S.-H.; Boreman, G.; Raschke, M. *Phys. Rev. B* **2012**, *86*, 235147.

(31) Kühler, P.; García de Abajo, F. J.; Solis, J.; Mosbacher, M.; Leiderer, P.; Afonso, C. N.; Siegel, J. *Small* **2009**, *5*, 1825−9.

(32) Mueller, J. P. B.; Capasso, F. *Phys. Rev. B* **2013**, *88*, 121410.

(33) Sönnichsen, C.; Franzl, T.; Wilk, T.; von Plessen, G.; Feldmann, J. *Phys. Rev. Lett.* **2002**, *88*, 077402.

(34) Radko, I. P.; Bozhevolnyi, S. I.; Evlyukhin, A. B.; Boltasseva, A. *Opt. Express* **2007**, *15*, 6576.

(35) Bozhevolnyi, S. I.; Volkov, V. S.; Devaux, E.; Laluet, J.-Y.; Ebbesen, T. W. *Nature* **2006**, *440*, 508−11.

(36) Sorger, V. J.; Oulton, R. F.; Ma, R.-M.; Zhang, X. *MRS Bull.* **2012**, *37*, 728−738.